Controlling Additive Behavior to reveal an Alternative Morphology Formation Mechanism in Polymer:Fullerene Bulk-heterojunctions

Nusret S. Güldal,[a]* Marvin Berlinghof,[b] Thaer Kassar, [b] Xiaoyan Du,[c] Xuechen Jiao,[d] Markus Meyer,[c] Tayebeh Ameri,[a] Andres Osvet,[a] Ning Li,[a] Giovanni Li Destri,[e] Rainer H. Fink,[c] Harald Ade,[d] Tobias Unruh,[b]* and Christoph J. Brabec[a]

a. Materials for Energy and Electronics, FAU Erlangen-Nürnberg, Martensstrasse 7, 91058, Erlangen, Germany
b. Chair for Crystallography and Structural Physics, FAU Erlangen-Nürnberg, Staudtstrasse 3, 91058, Erlangen, Germany
c. Physikalische Chemie, FAU Erlangen-Nürnberg, Egerlandstrasse 3, 91058, Erlangen, Germany
d. Department of Physics, North Carolina State University, Raleigh, NC 27695, USA
e. European Synchrotron Radiation Facility, 71 Avenue des Martyrs, 38000, Grenoble, France

Supplementary Information

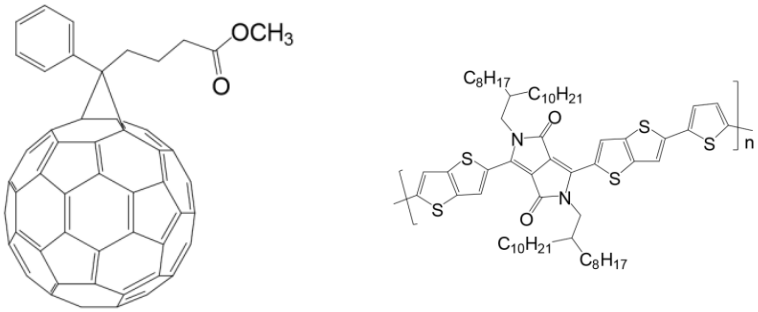

PCBM DPP-TT-T

Scheme. S1 Chemical structures of PCBM and DPP-TT-T.

Table S1. *Solar cell characteristic parameters presented for each sample measured.*

Sample	V_{OC}[V]	J_{SC} [mA/cm^2]	FF [%]	PCE [%]
w/o DIO	0.6	-4.47	46.79	1.25
1 vol% DIO + Eva	0.56	-6.32	53.37	1.89
2 vol% DIO	0.54	-11.03	59.25	3.53
2 vol% DIO + Eva	0.55	-13.89	61.36	4.68
4 vol% DIO + Eva	0.54	-8.48	68.08	3.12

BF-TEM (31K resolution)

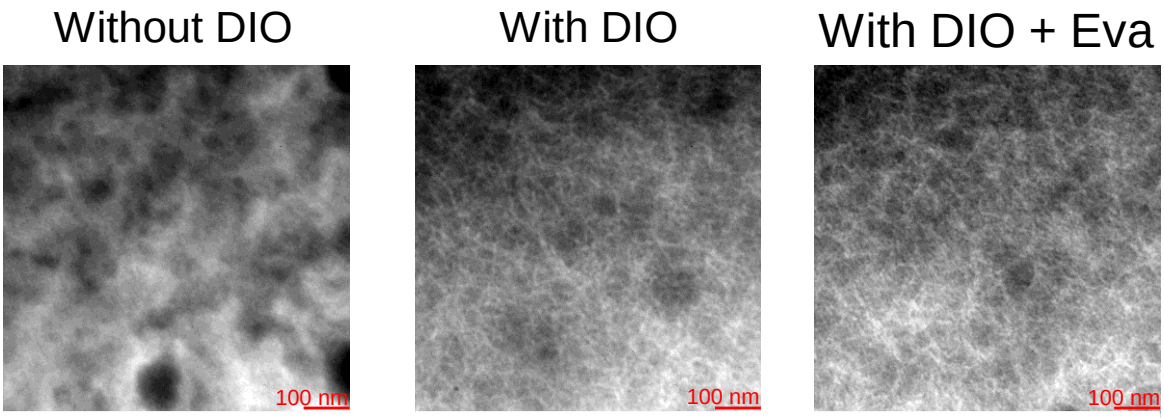

Fig. S1. BF-TEM pictures of additive-free DPP-TT-T:PCBM, DPP-TT-T:PCBM with 2 vol% DIO and DPP-TT-T:PCBM with 2 vol% DIO + Eva. Here, it is shown that additive-free sample has around 50 nm domains, while additive containing samples look very similar with domain size around 30 nm. This matches to the median characteristic lengths calculated from R-SoXS, as explained in main text.

R-SoXS Calculations

R-SoXS is measured in transmission geometry, and the lateral morphology is probed at a resonant energy which is characteristic to the electronic transition in the carbon atoms of organic molecules. The incident energy can be freely selected across the carbon 1s X-ray absorption in order to utilize vacuum contrast or material contrast. The proper energy should induce the maximum material contrast and should avoid the fluorescence background due to the strong PCBM absorption. For this purpose, as seen in Fig. S2, a range of energies was measured on DPP-TT-T:PCBM samples. At 270 eV, the vacuum contrast was dominating over the material contrast, while at other energies the material contrast was more dominant than vacuum contrast. Nevertheless, the fluorescence signal was observed at 285 eV as a result of strong PCBM absorption. In order to eliminate the fluorescence signal and receive high material contrast, 283.8 eV was chosen as the R-SoXS energy.

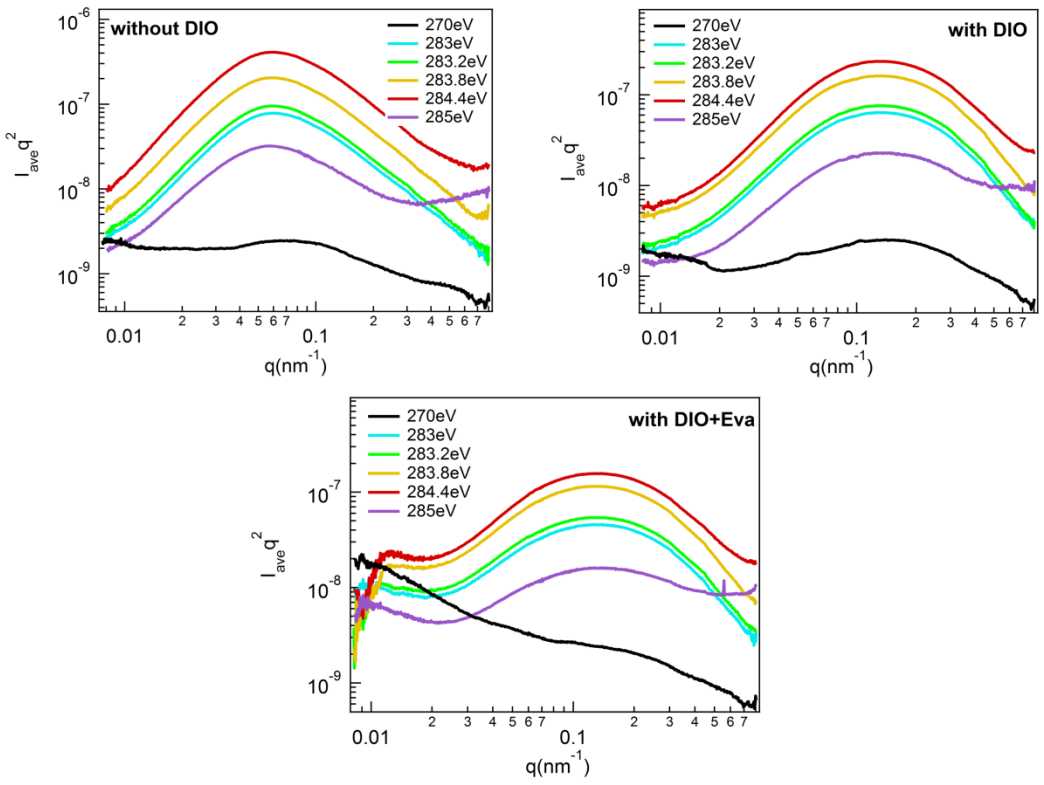

Fig. S2. R-SoXS scattering profiles of DPP-TT-T:PCBM without DIO (top left), with DIO (top right) and with DIO+EVA (bottom middle) at different energies. Vacuum contrast was dominant at 270 eV. The fluorescence background was observed at 285 eV, especially at high q range.

Resonant soft X-ray scattering (R-SoXS) was carried out at beamline 11.0.1.2 at ALS Lawrence Berkeley National Laboratory. All measurements were conducted under high vacuum (10^{-7} torr) to reduce the air absorption of soft X-rays. The samples were floated in deionized water and transferred on to Si_3N_4 substrates. The scattering patterns were collected by a 2048 pixels x 2048 pixels CCD detector. The data was processed with the Nika software package.[1] The information which can be collected from R-SoXS measurement includes: domain spacing (i.e. median characteristic length), relative average domain purity and molecular orientation. After the measurement, 180° azimuthal intensity averages (I_{avg}) were corrected by multiplying with q^2, leading to $I_{avg}q^2$ (i.e. Lorenz-corrected intensity).[2] Plotting $I_{avg}q^2$ vs q gives the reduced 1D data

from the original 2D data, as shown in Fig. 4 and S3. Integrated scattering intensity (ISI) is defined as the integration of the $I_{avg}q^2$ over the whole q range, shown in Equation S1. Since the scattering originates from the refractive index contrast between the domains (in this case, polymer-rich and fullerene-rich domains), the purer the domains are, the more intense scattering is measured. Hence ISI value is representative for relative domain purity:[3]

$$ISI = \int I_{avg} q^2(q) dq \tag{1}$$

The median characteristic length is calculated from the median spatial frequency, which is the q value equal to the half of the ISI (Equation S2).

$$d = \frac{2\pi}{q} \tag{2}$$

For polarized soft X-ray scattering (P-SoXS), anisotropy originates from the scattering intensity differences in the directions parallel and perpendicular to the X-ray polarization. Hence anisotropy ratio is calculated with the perpendicular and parallel polarized ISI values for each sample, shown in Equation S3:[3]

$$A \equiv \frac{ISI_{\perp} - ISI_{\parallel}}{ISI_{\perp} + ISI_{\parallel}} \tag{3}$$

Local chemical composition based on NEXAFS spectroscopy

NEXAFS spectra of the blends were taken by line scans (length: 4 μm, step width: 40 nm) in the region without large PCBM aggregations (mixed phase). The energy range was from 279 eV to 320 eV with 0.1 eV step in the energy range from 282 eV to 290 eV. X-ray optical density (OD) can be expressed by:

$$OD = \mu(h\nu)\rho d \tag{4}$$

where μ is absorption coefficient which depends on the respective chemical component and photon energy hν. ρ is the mass density of the respective component and d is the film thickness. For spectra deconvolution, optical densities of pristine DPP-TT-T and PCBM were normalized by post-edge (320 eV) and used as references. The local chemical composition ratio (Table S2) was computed using the aXis2000 software (McMaster Univ., Canada) by fitting the blend spectra (Fig. S3) to a sum of reference spectra using conjugate gradient optimization method, as in the following:

$$OD_{BLEND}(E) = \alpha_0 + \alpha_{DPP-TT-T} OD'_{DPP-TT-T}(E) + \alpha_{PCBM} OD'_{PCBM}(E) \quad (5)$$

where $OD_{BLEND}(E)$ is the X-ray absorption spectra of the blend film, $OD'_{DPP\text{-}TT\text{-}T}$ and OD'_{PCBM} the optical density of pristine DPP-TT-T and PCBM normalized to post edge and α_0, $\alpha_{DPP\text{-}TT\text{-}T}$, α_{PCBM} are the energy independent fitting parameters. Percentage chemical composition ratios were then determined by Equation S6 and S7:

$$\%\, DPP-TT-T = \alpha_{DPP-TT-T} \times \frac{100}{\alpha_{DPP-TT-T} + \alpha_{PCBM}} \quad (6)$$

$$\%\, PCBM = \alpha_{PCBM} \times \frac{100}{\alpha_{DPP-TT-T} + \alpha_{PCBM}} \quad (7)$$

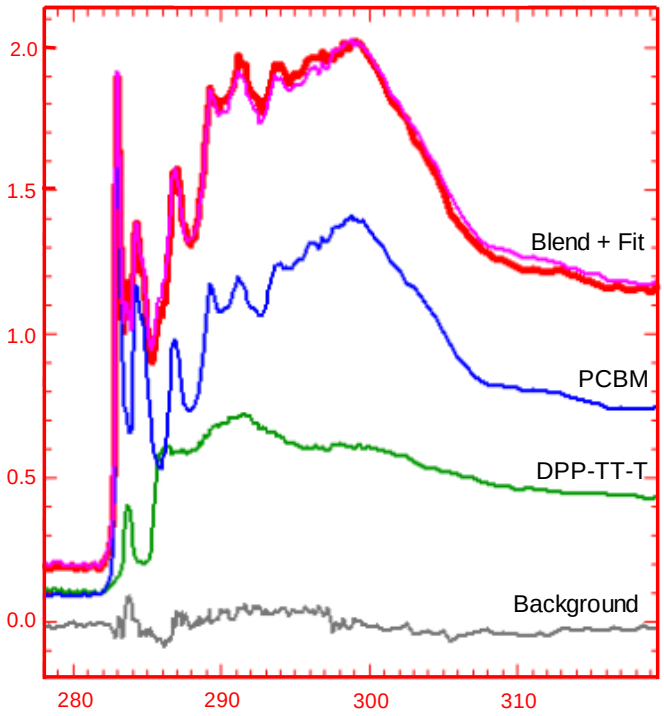

Fig. S3. Exemplary plot of NEXAFS spectra of pristine DPP-TT-T (green), pristine PCBM (blue) and additive-free DPP-TT-T:PCBM (red). The blend spectrum was fitted (pink) as explained above.

Table S2. *The summary of the local chemical composition ratio of the films*

Component	Additive-free	With DIO	With DIO + EVA
DPP-TT-T	37.5%	42.4%	40%
PCBM	62.5%	57.6%	60%

It should be noted that the preferential orientation of the polymer (i.e. film anisotropy) must not be overlooked during the chemical composition analysis. Although the GIXD results (Fig. 6a) indicated that there was not any strong orientation changes between the additive-free sample and DIO+Eva sample, the changes in the relative peak intensities for PCBM and DPP-TT-T are for

these samples very evident. Therefore, it can be concluded that composition variations affect the NEXAFS spectra more strongly than the anisotropy changes.

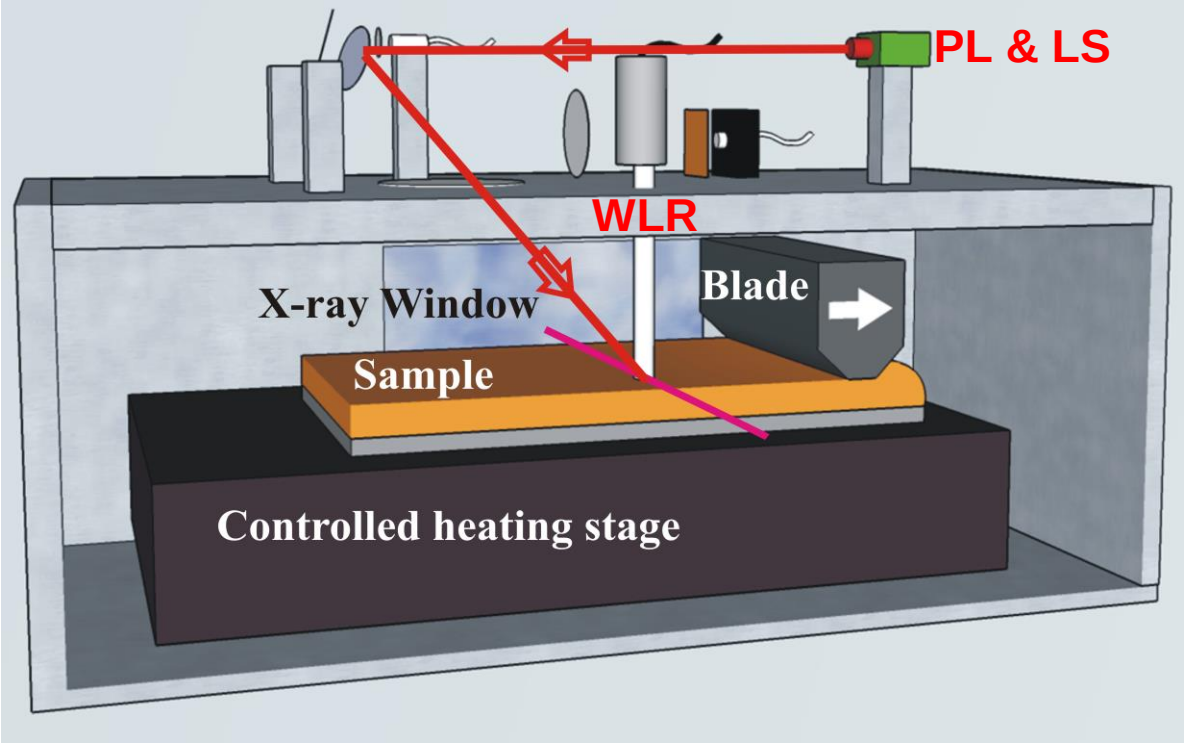

Fig. S4. Schematic of *in situ* measurement setup. Measurements are conducted on the same blading line, which is indicated by the pink line. This line is additionally the X-ray line at the beginning of each *in situ* measurement. Red lines with arrows indicate the PL/LS incidence geometry, which aligns directly on the WLR spot.

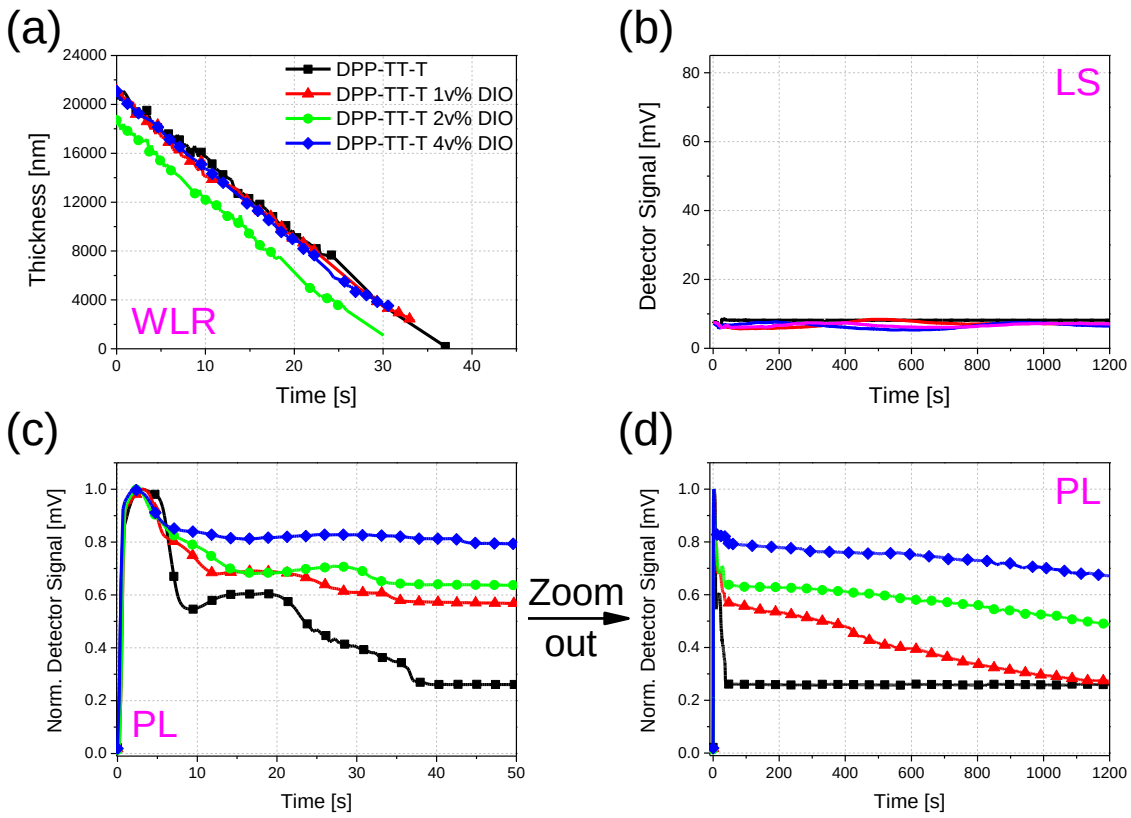

Fig. S5. Time evolution of pristine DPP-TT-T drying was measured by WLR (a), LS (b), PL (c) & (d). Figure (c) is additionally 'zoomed-out' (i.e. plotted over longer time scale), which is presented at figure (d). LS signal at (c) does not show any difference between the samples, as only background signal is present.

Table S3. *Solubility values for DPP-TT-T and PCBM, given in mg mL^{-1}*

Solvent	DPP-TT-T	PCBM
o-xylene	11	22.1[4]
mesitylene	0.2	22.5[4]
o-xy:mes	8	22.2
DIO	14	99.6[5]

Comparison of DIO effect on DPP-TT-T:PCBM system with P3HT:PCBM and PffBT4T-2OD:PCBM blends

Poly(3-hexylthiophene) (P3HT) is one of the most studied blend systems in literature in terms of additive effects on the microstructure, especially with *in situ* methods. It is known that additives like octanedithiol (ODT) and DIO are non-solvents for P3HT, leading towards an early aggregation of P3HT, by degrading host solvent quality.[6] Even the additives which are good solvents for P3HT, like 1-chloronapththalene (CN), promote early aggregation of P3HT since CN is not a better solvent for the polymer than the conventional solvents used as host solvents. The solubility of P3HT in CN is not high enough to induce a drying behavior close to thermodynamic equilibrium.[7] In order to compare the effect of DIO on the drying behavior of DPP-TT-T:PCBM system, we have measured P3HT:PCBM in chlorobenzene without and with 3 v% DIO, coated under same conditions (Fig. S6), As expected, DIO does not induce any thermodynamic equilibrium behavior on P3HT:PCBM. Especially the PL data confirms the fact that DIO does not cause higher signals than the PL signal of additive-free P3HT:PCBM right after host solvent drying, indicating that the aggregation/crystallization of the P3HT is not delayed under the presence of DIO, as it was observed with DPP-TT-T (Fig. 7c & Fig. S5c).

Another comparison was made with the best performing polymer:fullerene system so far, PffBT4T-2OD:PCBM, whose aggregation/crystallization behavior is strictly controlled by 3 v% DIO and high temperature coating and drying.[8] It has been recently shown that PffBT4T-2OD experiences strong nucleation and aggregation when processed at approximately 60 °C from CB:ODCB mixture with 3 v% DIO.[8] Here, we present the *in situ* drying data of PffBT4T-2OD:PCBM, coated and dried under same conditions. Although DIO most likely causes nanoscale differences in the domain sizes, degree of phase separation and crystal size, the microstructure evolution (Fig. S7) is not hindered or delayed under its presence. LS and PL

signals for the samples with and without DIO do not show any indication that DIO causes a similar drying behavior as it shows with DPP-TT-T:PCBM system.

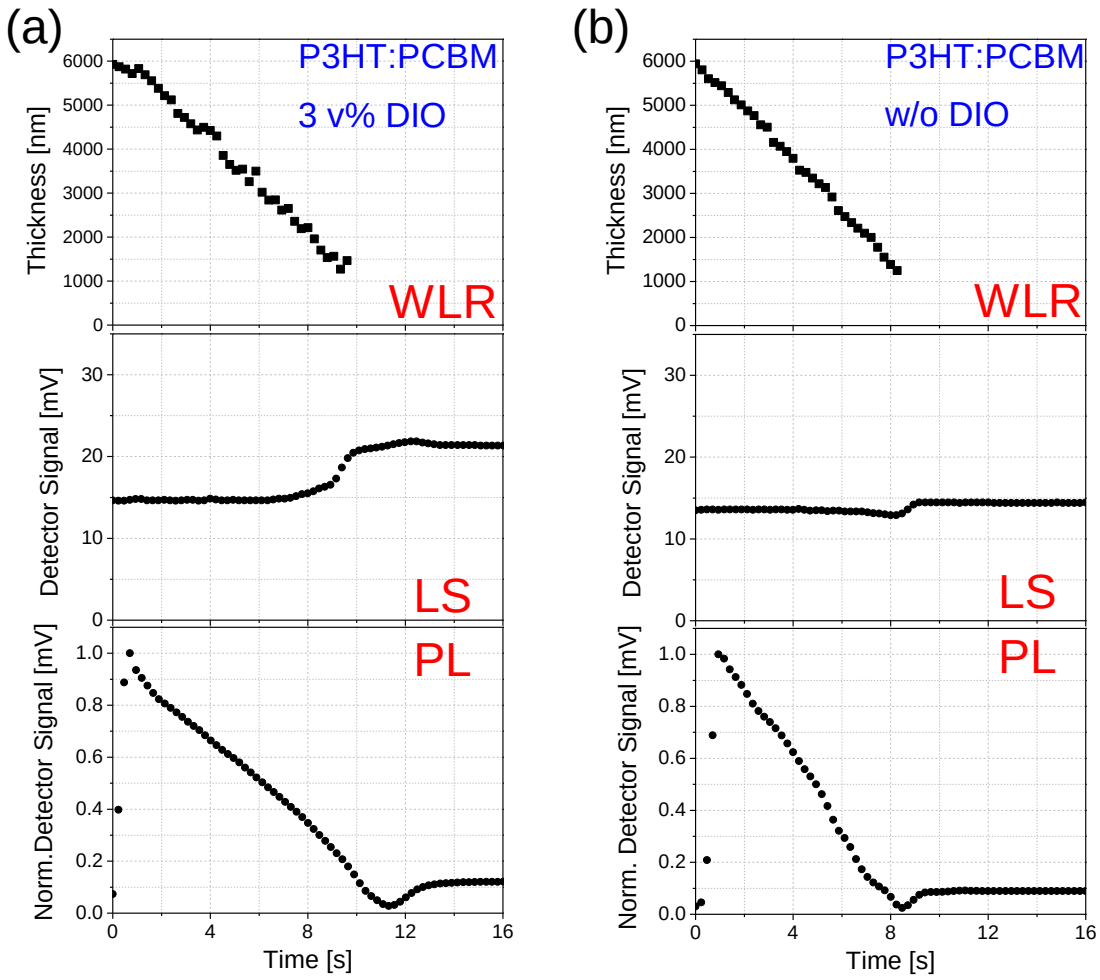

Fig. S6. Drying evolution of P3HT:PCBM with (a) and without (b) 3 v% DIO was measured by WLR, LS and PL. WLR data for both samples show constant rate drying. LS signal for the sample with additive shows higher intensity after CB-drying than the sample without additive. This is probably due to slightly bigger aggregates forming in the presence of DIO. PL data does not show any difference between additive-free and additive-containing P3HT:PCBM layers. Hence, the self-quenching mechanism due to the polymer aggregation/crystallization is not hindered by DIO, unlike DPP-TT-T:PCBM.

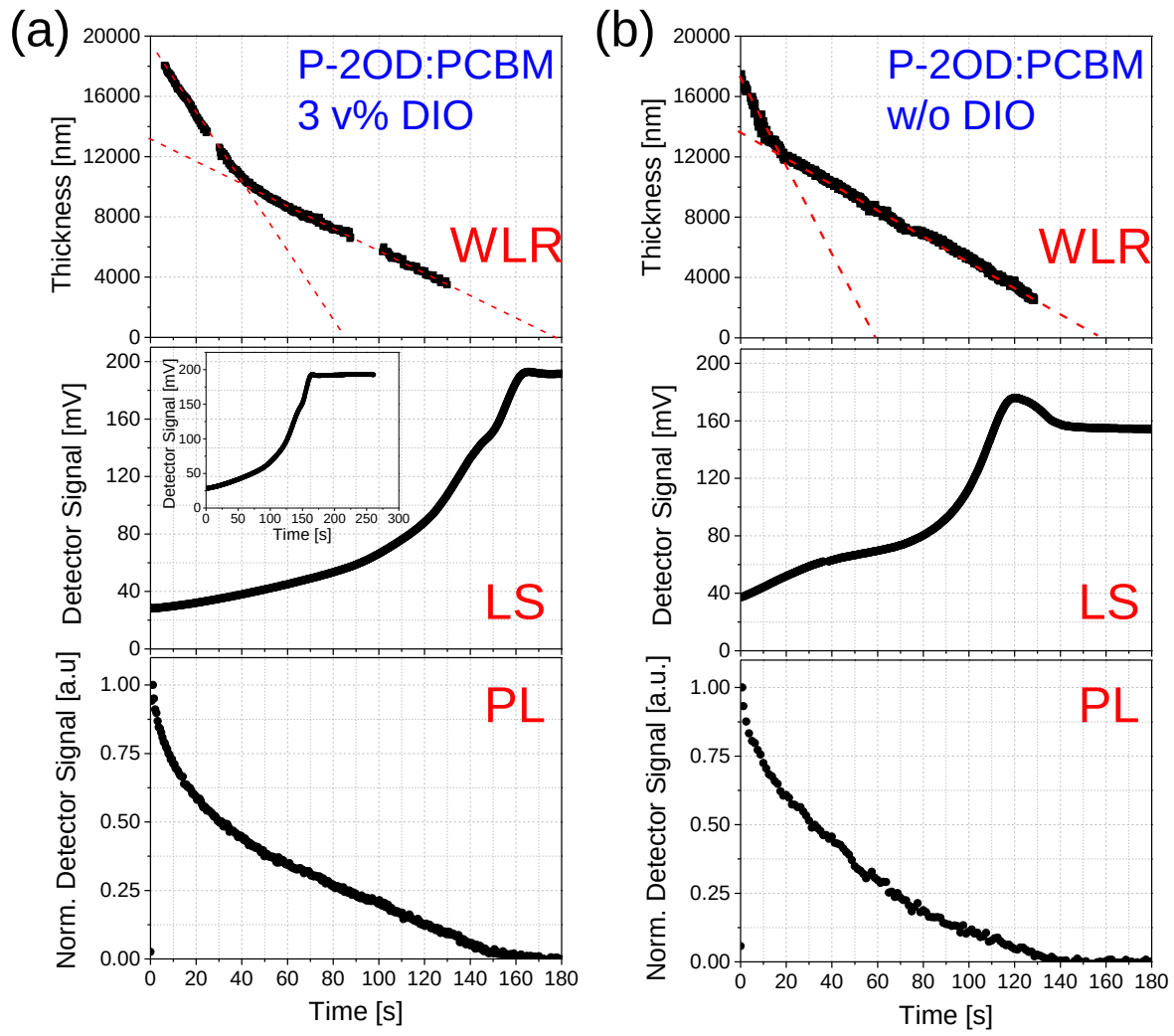

Fig. S7. Drying evolution of PffBT4T-2OD:PCBM with (a) and without (b) 3 v% DIO was measured by WLR, LS and PL. P-2OD is the short version of PffBT4T-2OD used on the plots due to limited space. The inset at (a) LS plot is plotted over extended period of time in order to indicate that the LS signal stays constant after 170th second. WLR data for both samples indicate two drying rates for the host solvent drying: CB-dominated drying at early stage and ODCB-dominated drying at later stage. LS signal increases constantly over the whole host solvent drying period, fitting to the description of PffBT4T-2OD with very rapid aggregation. PL signal is not influenced by the additive as it only shows a very rapid quenching, caused by a combination of aggregation quenching and quencher effect.

Drying behavior of DPP-TT-T:PCBM and pristine DPP-TT-T processed from ODCB-based solution with and without DIO

It can be argued that this extraordinary DIO effect on DPP-TT-T:PCBM is only observable because of the suboptimal solvent mixture (o-xylene:mesitylene) used for the blend. We have additionally measured the drying behavior of DPP-TT-T:PCBM in CB without any additive and with 1, 2 and 4 v% DIO. With CB, it is expected that the drying becomes more homogenous. Especially the gelation behavior caused by o-xylene (seen by PL) and the formation of big PCBM aggregates caused by mesitylene (seen by LS) are hindered as soon as CB is taken as the host solvent (Fig. S8). Instead, DPP-TT-T was showing a high LS signal due to aggregation.

With regarding the DIO effect on the evolution of polymer aggregation/crystallization, although the solubility in CB is presumably higher than it is in DIO, CB dries faster than DIO due to higher vapor pressure; hence the additive would still keep most of the polymer dissolved, i.e. hindering polymer aggregation/crystallization. This is confirmed by the PL measurements of DPP-TT-T:PCBM and pristine DPP-TT-T from CB with different amounts of DIO, presented in Fig. S8a and S8b. As the PL signals stay stronger than the additive-free samples, it can be deduced that the PL quenching is partially prohibited due to the reduced polymer aggregation/crystallization under the DIO presence. This behavior is similar to the PL behavior of DPP-TT-T:PCBM processed from o-xylene:mesitylene mixture (Fig. 7).

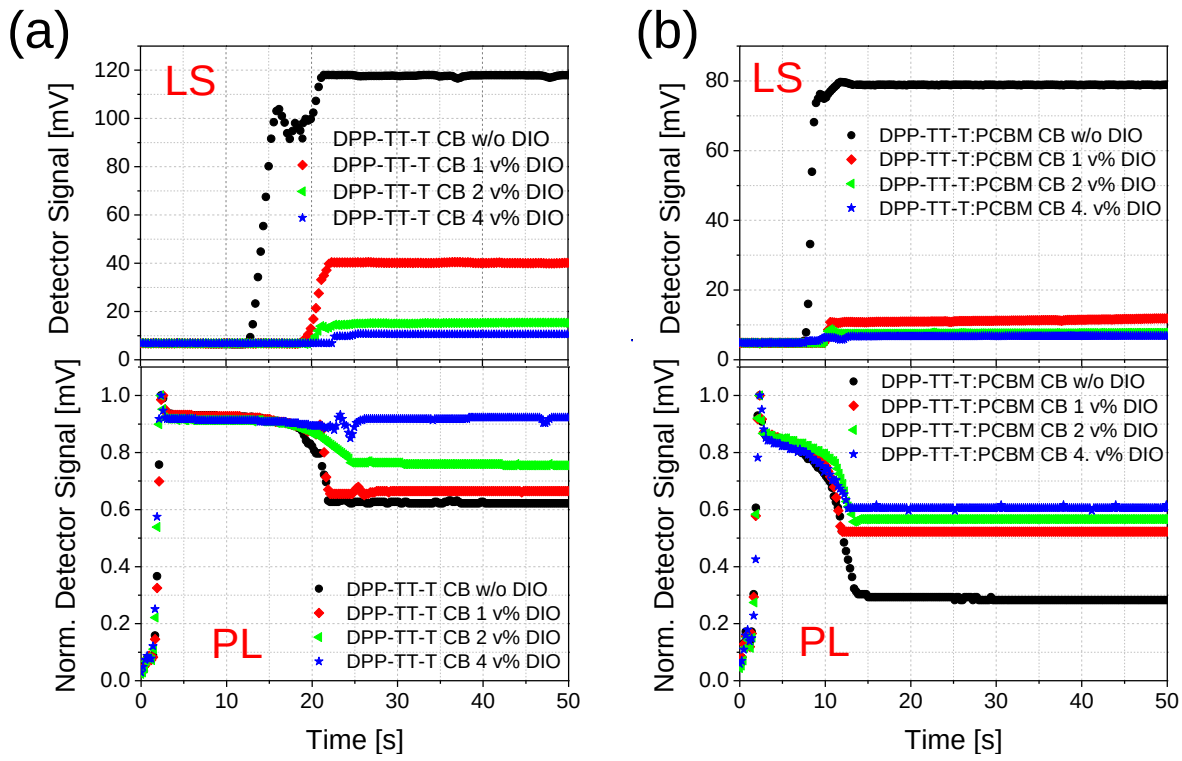

Fig. S8. Drying evolution of pristine DPP-TT-T (a) and DPP-TT-T:PCBM (b) processed from CB without and with 1, 2 and 4 v% DIO.

Summary on calculation of thickness from white-light reflectometry

Thickness values from reflectance spectrum for each sample were calculated based on the interference theory. Example spectrum of DPP-TT-T:PCBM on Si wafer with natural SiO_2 layer are presented in the following:

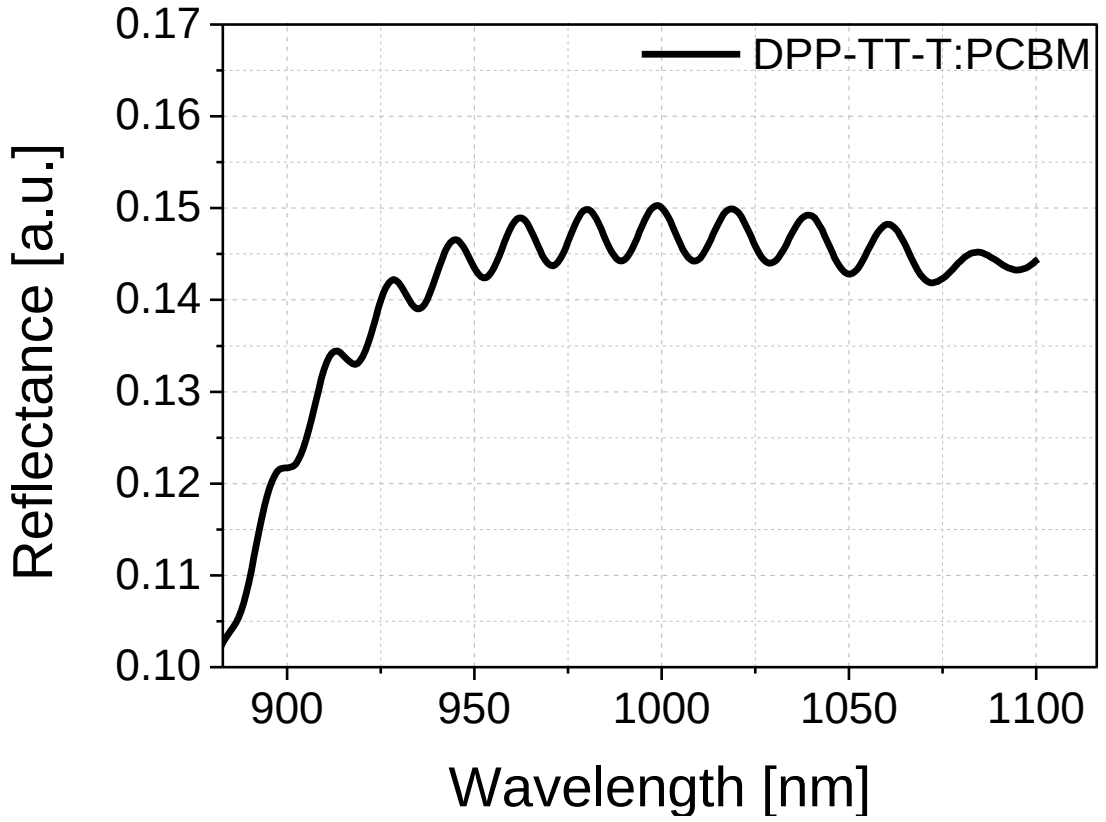

Fig. S9. An example reflection spectrum of additive-free DPP-TT-T:PCBM on Si wafer with natural SiO_2 during drying

Theoretically as the thickness reduces, fringes would be also observed at higher energy regions. Thickness calculations in these regions (UV-900 nm for DPP-TT-T:PCBM) should be conducted very carefully since these regions contain several different information (Si wafer reflectance, Si wafer absorption, coated film absorption, reflection of the layer surface, interference fringes…). Firstly, some of these effects damp the interference fringes heavily, and secondly, absorption information of the coated film is not reliable for any sort of comparison.

Therefore, the wavelength range (IR) for thickness calculations was selected in a way that these effects are minimized. In the IR region, we only have Si wafer absorption, which reduces the signal, but not disturbing interference fringes.

For a reflection of a film on a substrate with higher refractive index, superposition of two reflected waves can have two distinct cases with respect to the path difference:

$$\Delta_{const.} \rightarrow 2dn = m\lambda$$
$$\Delta_{destr.} \rightarrow 2dn = (m + \frac{1}{2})\lambda \quad (8)$$

where λ is the wavelength, d is film thickness, and n is refractive index. Based on these equations, film thickness for a layer which has different refractive indices at different wavelengths can be calculated from two adjacent maxima (or minima) as in the following:

$$d = \frac{\lambda_1 \lambda_2}{2(\lambda_1 n_2 - \lambda_2 n_1)} \quad (9)$$

This calculation is very accurate if the refractive indices are handled correctly. For this manuscript, we calculated the dielectric function of DPP-TT-T:PCBM solutions at different concentrations via Effective Medium Approximation (Bruggeman). Dielectric functions of the solvents and dried layer of DPP-TT-T:PCBM were measured with spectroscopic ellipsometry (Woollam M-2000). Effective Medium Approximation was then conducted in commercially available software WVASETM. It should be noted that, close to the final drying (from 30th second on and DIO-drying), thickness values cannot be calculated due to interference losses. These losses occur due to the strong changes in the dielectric functions of these blends close to the drying, especially due to their anisotropic character. These regions can be resolved and modelled by ellipsometry properly, when it is needed. Although we cannot resolve these drying regions with reflectometry measurements, the time point for the end of drying can be recognized as the time point at which the spectrum stops changing.

1 J. Ilavsky, *J. Appl. Crystallogr.*, 2012, **45**, 324–328.

2 N. Stribeck, *X-Ray Scattering of Soft Matter*, Springer Berlin Heidelberg, Berlin, Heidelberg, 2007, vol. 1.

3 J. R. Tumbleston, B. a. Collins, L. Yang, A. C. Stuart, E. Gann, W. Ma, W. You and H. Ade, *Nat. Photonics*, 2014, **8**, 385–391.

4 F. Machui, S. Langner, X. Zhu, S. Abbott and C. J. Brabec, *Sol. Energy Mater. Sol. Cells*, 2012, **100**, 138–146.

5 F. Machui, P. Maisch, I. Burgues-Ceballos, S. Langner, J. Krantz, T. Ameri and C. J. Brabec, *ChemPhysChem*, 2015, **16**, 1275–1280.

6 N. Shin, L. J. Richter, A. A. Herzing, R. J. Kline and D. M. DeLongchamp, *Adv. Energy Mater.*, 2013, **3**, 938–948.

7 L. J. Richter, D. M. Delongchamp, F. A. Bokel, S. Engmann, K. W. Chou, A. Amassian, E. Schaible and A. Hexemer, *Adv. Energy Mater.*, 2015, **5**, 140975.

8 H. W. Ro, J. Downing, S. Engmann, A. Herzing, D. Delongchamp, L. Richter, S. Mukherjee, H. Ade, M. Abdelsamie, A. Amassian, L. K. Jagadamma, H. Yan and Y. Liu, *Energy Environ. Sci.*, 2016.